Journal of Nuclear Medicine, published on January 10, 2020 as doi:10.2967/jnumed.119.237891

Immune checkpoint imaging in oncology – a game changer towards personalized immunotherapy?

Running title: Checkpoint imaging in oncology

Dr. Dr. Susanne Lütje[1], PD Dr. Georg Feldmann[2], Prof. Dr. Markus Essler[1], Prof. Dr. Peter Brossart[2], Prof. Dr. Dr. Ralph A. Bundschuh[1]

[1] Department for Nuclear Medicine, University Hospital Bonn, Germany

[2] Department of Internal Medicine 3, Center of Integrated Oncology (CIO) Cologne-Bonn, University Hospital Bonn, Germany

Disclaimer: No conflicts of interest exist.

Corresponding author:

Dr. Dr. Susanne Lütje (resident)

University Hospital Bonn

Department for Nuclear Medicine

Venusberg-Campus 1

53127 Bonn

Germany

Susanne.Luetje@ukbonn.de

Word count: 6325 (without references 4089)

ABSTRACT

Immune checkpoint blockade represents a promising approach in oncology, showing anti-tumor activities in various cancers. However, although being generally far more well-tolerated than classical cytotoxic chemotherapy, this treatment, too, may be accompanied by considerable side effects and not all patients benefit equally. Therefore, careful patient selection and monitoring of the treatment response is mandatory. At present, checkpoint-specific molecular imaging is increasingly investigated as a tool for patient selection and response evaluation. Here, an overview of the current developments in immune checkpoint imaging is provided.

KEY WORDS

Checkpoint blockade, molecular imaging, Oncology, PET/CT

INTRODUCTION

The basic idea of cancer immunotherapy is to induce, potentiate, and revive anti-tumor responses originating from a patient´s immune system. Depending on the amount of mutations in cancer cells, immune cells are able to recognize and attack cancer cells. However, evasion of attack by the immune system is one of the hallmarks of cancer, leading to the development of tolerance (*1*). This process can be initiated by several mechanisms, including the upregulation of inhibitory immune checkpoint pathways, such as the programmed cell death protein 1 (PD-1)/programmed death-ligand 1 (PD-L1) or cytotoxic T lymphocyte-associated protein 4 (CTLA-4) (*2,3*). T-cell effector function can be downregulated by these pathways, which may lead to tumors evading immune surveillance. Immune checkpoint inhibitors targeting one of these pathways inhibit these immune escape mechanisms and thereby re-activate the immune system to recognize and destroy the tumor cells.

So far, several of such immune checkpoint inhibitors are registered and approved for cancer treatment, including anti-CTLA-4 antibodies such as ipilimumab (*4*), anti-PD-1 antibodies such as nivolumab (Opdivo) (*5*) or pembrolizumab (Keytruda) (*6*), as well as anti-PD-L1 antibodies such as durvalumab (Imfinzi) (*7*), avelumab (Bavencio) (*8*) or atezolizumab (Tecentriq) (*9*). Encouraging results have been reported in various malignancies including melanoma, breast cancer, head and neck cancer, as well as non-small cellular lung cancer (NSCLC), where immune checkpoint blockade is currently complementing classical cytostatic chemotherapy as a first-line therapy in certain subsets of patients (*10*). Despite impressive clinical responses in a series of malignancies so far, the reality remains that these responses are limited to defined patient subgroups. In consequence, non-responding patients may unnecessarily be exposed to these regimens posing the risk of potential associated adverse effects, which may include severe immune-related adverse events, such as pneumonitis, colitis, or pancreatitis (*11-13*). Therefore, there is a pressing need for biomarkers to identify patients who will respond to and profit from immune checkpoint blockade in oncology.

IMMUNE CHECKPOINT BLOCKADE

At present, immune checkpoint blockade for two pathways is clinically most commonly used, one interfering with the PD-1/PD-L1 axis, and the other one involving CTLA-4. Therefore, first, a short overview of these two pathways is presented.

PD-1/PD-L1 pathway

PD-1 is an immunosuppressive cell surface receptor expressed on immune cells, including activated T-cells, regulatory T-cells, B-cells, natural killer cells, activated monocytes, and dendritic cells (*14*). PD-L1, one of the ligands of PD-1, is expressed on a wide range of malignancies such as lung cancer(*15*), melanoma (*16*), and renal cells carcinoma (*17*), as well as on resting T-cells, B-cells, dendritic cells, macrophages, vascular endothelial cells and pancreatic islet cells (*14*). For T-cells to be activated, two signals are required. First, interaction between the antigen-major histocompatibility complex and the T-cell receptor on T-cells needs to present. Secondly, a co-stimulatory signal provided by antigen-presenting cells (APCs) is needed. Once the T-cells are activated, T-cell clonal expansion, cytokine secretion, and T-cell effector function is initiated. Binding of PD-1 to PD-L1 inhibits the co-stimulatory signal, which leads to T-cell dysfunction, allowing tumor cells to evade the anti-tumor immune response (**figure 1 a**).

CTLA-4 pathway

Another key inhibitory immune checkpoint is CTLA-4. CD28, which is expressed on resting and activated T-cells, works as a co-stimulatory receptor and promotes T-cell proliferation and effector function upon binding its ligand B7 on APCs. CTLA-4 is homologous to CD28 and shares the same B7 ligand, but negatively effects T-cell activation. While resting T cells rarely express CTLA-4, CTLA-4 is upregulated after T-cell receptor (TCR) activation and binds B7 with a higher avidity than CD28, resulting in reduced T-cell proliferation. In addition, regulatory T-cells control functions of effector T-cells, and thus are key players in maintaining peripheral tolerance, as regulatory T-cells constitutively express CTLA-4, which is

thought to be important for their suppressive functions (*3*). Recently, CTLA-4 was found to be expressed on various malignant tissues (*18-25*) and correlates with outcome in certain cases (*21,23,26*). Upregulation of CTLA-4 by tumor cells may prevent APCs from presenting tumor-associated antigens (TAAs) to naive T-cells. Consequently, T-cell activation and tumor destruction can be prevented (**figure 1b**). Ipilimumab, an anti-CTLA-4 antibody, was approved by the Food and Drug Administration in 2011 for treatment of metastatic and high-risk resected melanoma and has been shown to be effective in multiple phase II/III trials (*27*).

ROLE OF IMAGING OF IMMUNE CHECKPOINT BLOCKADE

In the oncological setting, imaging including computed tomography (CT), magnetic resonance imaging (MRI), and positron-emission tomography (PET)/CT is applied for three main reasons: 1. staging/patient selection, 2. evaluating treatment responses, 3. monitoring/follow-up after therapy. As immune checkpoint blockade is an expensive treatment which can have severe side effects, careful patient selection is of great importance.

While conventional imaging methods such as CT and MRI are mainly limited to anatomical/functional assessment of a patient`s tumor load, PET provides us with the possibility for molecular functional imaging. Recent reports have highlighted the potential of ^{18}F-fluorodeoxyglucose (FDG)-PET/CT for the assessment of responses to immunotherapies (*28,29*). However, its role in predicting responses prior to administration of the therapy to optimize patient selection remains yet to be determined. Also, some initial data suggest, that the FDG uptake before initiation of treatment with nivolumab or pembrolizumab may have some predictive value to the treatment outcome (*30*). While for immunotherapies only limited data is available this potential use of PET is well known in other treatments as chemotherapy or external beam radiation. E.g. can PET features in the pretherapeutic

PET/CT predict the response to neoadjuvant treatment of rectal cancer (*31*). Similar results were found e.g. in esophageal cancer (*32,33*) or neuroendocrine tumors using somatostatine receptor PET (*34*).

At present, patient selection is mainly based on immunohistochemical analysis of biopsy material. Unfortunately, this approach has several limitations. First, expression levels and the invasion of tumor-infiltrating lymphocytes changes over time due to alterations in the tumor microenvironment or in response to treatments (*35-41*). Secondly, expression levels can be very heterogeneous within and between tumor lesions. Therefore, even though biopsy specimens may express high levels of PD-L1 at a given point in time, the majority of the lesions in the patient may actually be negative for these markers, which may lead to misinterpretation of the overall PD-L1 status, if only a single biopsy specimen is analyzed (*42-48*).

To overcome these limitations, target-specific tracers for real-time *in vivo* imaging are currently under investigation, which may have great potential to improve patient selection prior to immune checkpoint blockade therapy (**figure 2**).

PRECLINICAL ADVANCES IN IMMUNE CHECKPOINT IMAGING

Imaging of PD-L1 expression

Currently, the major part of the checkpoint imaging studies have focused on visualizing PD-L1 expression, whether on tumor cells or in the tumor microenvironment. Among these studies, various targeting molecules have been evaluated, however, antibody molecules were most frequently used.

PD-L1 imaging based on antibody molecules

So far, a series of preclinical studies has shown feasibility to specifically visualize PD-L1 expression using radiolabeled anti-PD-L1 antibodies for PET or SPECT imaging (**table 1**). Specific tracer uptake with high tumor-to-background contrast was reported for various PD-L1-expressing xenografts, with low uptake in PD-L1-negative tumors (*49-51*). In addition, graded levels of PD-L1 expression were shown to be

detectable in different human tumor xenografts (CHO-PDL1, MDA-MB-231, H2444) (*50*) and intra-tumoral heterogeneity could be visualized (*52*). One disadvantage of xenograft tumor models is the fact that immunodeficient mice are needed. In consequence, expression of PD-L1 on healthy organs and immune cells cannot be evaluated. In an effort to overcome this, immunocompetent mice with murine tumors are being used increasingly, together with anti-murine anti-PD-L1 antibodies as targeting molecules. Besides high uptake of the radiolabeled anti-PD-L1 antibodies in tumor tissue, tracer uptake in healthy PD-L1-expressing tissues such as brown fat, spleen, liver, thymus, heart, and lungs was reported (*53*).

Another important consideration is the impact of protein concentration on the distribution of radiolabeled anti-PD-L1 antibodies. Nedrow et al. observed an increasing tumor uptake with escalating tracer doses, which the authors hypothesized may be due to the spleen acting as a sink for the anti-PD-L1 antibody (*54*). To enhance uptake in tumors, a therapeutic dose of unlabeled anti-PD-L1 antibody was added to the tracer dose of ^{111}In-DTPA-anti-PD-L1 to block PD-L1 binding sites in the spleen. In this study, a dose of 3 mg/kg antibody led to optimal biodistribution and tumor-to-background ratios. The hypothesis, that it is possible to monitor the impact of PD-L1-rich organs on the distribution of anti-PD-L1 antibodies, was confirmed (*54*).

Other than ^{111}In (SPECT), anti-PD-L1 antibodies have been labeled to radioisotopes such as ^{64}Cu or ^{89}Zr for PET imaging applications (*55,56*). Lesniak and colleagues evaluated the anti-PD-L1 antibody atezolizumab labeled with ^{64}Cu using the chelator DOTAGA for PET imaging of PD-L1 expression, showing high tracer uptake in PD-L1-expressing tumors (*57*). Recently, a DOTAGA-chelated, ^{111}In-labeled anti-HER3 affibody carrying a negative charge at the C-terminus was shown to have significantly lower liver uptake compared to the ^{111}In-labeled NOTA-chelated variant (*58*). However, this observation has not yet been confirmed for anti-PD-L1 antibodies, but this should be evaluated in order to optimize the biodistribution profile of these antibodies regarding sink effects of the liver.

The majority of the above described studies focused on developing approaches to visualize PD-L1 expression with SPECT or PET and to further optimize these imaging approaches by varying the protein dose, the used radioisotope, or the chelating molecule. In addition to pure a priori visualization of the checkpoint expression status in oncologic patients, knowledge on the impact of different therapies on the expression status would be desirable. Hettich et al. evaluated the effect of IFN-y treatment on PD-L1 expression. They found that PD-L1 expression in mice with wild-type B16F10 melanomas was augmented upon IFN-y treatment and were able to visualize this. Kikuchi et al. provided evidence that radiotherapy induces changes PD-L1 expression which could be visualized with PET/CT imaging (*59*). Radiotherapy was able to induce an upregulation of PD-L1 on B16F10 melanoma cells, which may affect the response to PD-L1-based checkpoint blockade therapy. However, this upregulation is a dynamic process that has been difficult to monitor during treatment in the clinical situation. In this particular study, PET/CT performed at 48 h or 96 h post injection was suitable for confirming PD-L1 increases in irradiated tumors before the commencement of immune checkpoint therapy or other interventions. Feasibility to visualize radiotherapy-induced changes of PD-L1 expression was confirmed by other groups using SPECT with ^{111}In-labeled anti-PD-L1 antibodies (*52*) or PET using ^{89}Zr-labeled tracers (*60*). In the latter study, increases in PD-L1 expression from baseline were observed in H460 cells after daily radiotherapy of 5 fractions of 2 Gy and could be visualized in vivo with ^{89}Zr-Df-atezolizumab PET imaging. Interestingly, a statistically significant higher tracer accumulation was reported in fractionated H460 tumors as compared to all other H460 groups.

PD-L1 imaging based on smaller targeting molecules

One limitation of the described studies on checkpoint imaging is the fact that full-length IgG antibodies were used (~150 kDa), which due to their size may have limited tissue and tumor penetrance. Therefore, the time interval between tracer injection and imaging needs to be long enough and corresponding

radioisotopes such as ^{111}In or ^{64}Cu need to be used, resulting in increased radiation dose and more complex clinical protocols.

In an effort to improve this for PD-L1 imaging, Li et al. evaluated an 80 kDa anti-human PD-L1 domain antibody containing Fc tail fused to two single domains, labeled to ^{89}Zr via DFO (*61*), hoping to obtain improved tumor penetration and tumor-to-background ratios at earlier time points than monoclonal antibodies. Indeed, high tumor-background contrast was observed at 24h postinjection.

Other approaches towards fast target accumulation and rapid clearance of unbound tracer include the use of even smaller targeting molecules such as Fab fragments like ^{64}Cu-NOTA-anti-PD-L1-Fab (*62*), which retain the binding of antibodies but lack the Fc effector domain, leading to altered pharmacokinetics including shorter circulation-half lives. Besides Fab fragments (~55 kDa), checkpoint imaging using small-molecules including ^{99m}Tc- and ^{68}Ga-labeled nanobodies (~15 kDa), ^{18}F-labeled adnectins (~ 10 kDa), ^{18}F-AlF-labeled affibodies (~6 kDa) and peptides (<1 kDa) has been investigated (*63-69*). Due to the small size of these targeting molecules as compared to antibody molecules, these agents are delivered rapidly to their targets with fast clearance und the unbound probe, providing high image-contrast. In addition, some of these targeting molecules, such as adnectins, are very stable and the absence of cysteine or disulfide bonds allows the introduction of a single cysteine for site-specific conjugation of radioisotopes. In vivo imaging indeed revealed rapid delivery of these tracers to PD-L1–expressing tumors and rapid clearance from non-PD-L1–expressing tumors and tissues. Compared to intact antibody molecules, which are not cleared renally but via the hepatic route, smaller targeting molecules (depending on their size) are often cleared via the kidneys, which should be considered when tumor lesions in the vicinity of these organs need to be evaluated.

The anti-PD-L1 peptide WL12 labeled to ^{64}Cu or ^{68}Ga was shown to detect tumor PD-L1 expression specifically and rapidly after injection of the radiotracer, which fits within the standard clinical workflow of imaging within 60 min of administration (*67,68*). Subsequently, the preparation of a radiofluorinated analog of WL12 using 2,3,5,6- tetrafluorophenyl 6-^{18}F-fluoronicotinate was reported

(*69*). Fluorine-18 is well suited for clinical translation with 97% decay via positron emission and a half-life of 109.8 minutes, allowing transportation of the radiotracer from the regional radiopharmacy to the clinical site. In vivo data demonstrated a PD-L1-specific uptake of ^{18}F-FPy-WL12 in a series of tumors on NSG mice. In addition to PD-L1-expressing tumors, high accumulation of the tracer was observed in liver and kidneys, which could not be blocked, suggesting a non-specific accumulation of the radiotracer in these organs.

Taken together, these data show that several alternatives for intact IgG molecules are available and are currently being tested for checkpoint imaging purposes. So far, the first results look promising and even tracers for PET become available, which will stimulate further research towards clinical translation. These tracer alternatives are particularly interesting regarding their small size and fast clearance profiles which imply that imaging can be performed as early as minutes to hours post injection. Together with the advantages in practical work flows in the clinical situation, using smaller targeting agents also limits the amount of time patients are exposed to radioactivity.

Imaging of PD-1 expression

Previously, a correlation between response to PD-1 checkpoint blockade and presence of PD-1-expressing TILs has been shown (*45,70*). So far, several studies have focused on the development of PD-1 specific imaging approaches to visualize PD-1 expressing T-cells in the tumor microenvironment as well as in immune tissues. While several targeting molecules (including antibodies, antibody fragments and small molecules) were tested for PD-L1 imaging so far, PD-1 imaging was almost exclusively performed with IgG molecules including ^{64}Cu-DOTA-anti-PD-1 (*71*), ^{64}Cu-NOTA-anti-PD-1 (*55*), ^{89}Zr-DFO-nivolumab (*72*), ^{89}Zr-Df-nivolumab (*73*), and ^{89}Zr-Df-pembrolizumab (*74,75*). Besides visualization of PD-1-expressing tumor-infiltrating lymphocytes in the tumor microenvironment, specific uptake was observed in the spleen and lymph nodes, which is due to PD-1-expression in lymphocytes. In addition, salivary and lacrimal gland infiltration of T-cells was reported (*73*). Taken together, these findings support the idea

that PD-1-specific PET imaging may contribute to patient selection as it may have potential to aid in predicting response to therapies targeting immune checkpoints and become a tool for disease monitoring.

Imaging of CTLA-4 expression

One of the first immune checkpoints that have been targeted for checkpoint blockade therapy is CTLA-4 (*76*). Ehlerding et al. investigated the potential of CTLA-4 as a target for PET imaging and were able to visualize CTLA-4 expression on NSCLC with ^{64}Cu-DOTA-ipilimumab PET/CT (*22*) and ^{64}Cu-NOTA-ipilimumab PET/CT in humanized mouse models (*77*). In addition, a ^{64}Cu-labeled F(ab´)$_2$ fragment of ipilimumab was assessed for PET imaging of CTLA-4 expression on T cells. ^{64}Cu-NOTA-ipilimumab demonstrated high absolute uptake in the salivary glands of the humanized mice, which the authors attribute to a result of graft-versus-host-disease. In contrast, ^{64}Cu-NOTA-ipilimumab-F(ab')$_2$ uptake was lower. However, rapid clearance from the circulation was observed for the F(ab')$_2$ agent, leading to higher salivary gland-to-blood ratios.

In summary, whether using IgGs or smaller fragments as targeting molecules, visualization of CTLA-4 expression seems feasible.

OTHER IMAGING TARGETS

Kelly et al. assessed the fully human antibody REGN3767 radiolabeled with ^{89}Zr using the bifunctional chelator DFO which is directed against the lymphocyte-activation gene 3 (LAG-3) (*78*). Lag-3 is an immune checkpoint target expressed by activated T lymphocytes, which reduced T cell function (*79*). Lag-3-expressing TILs are correlated with large mass volume of malignancies, high proliferation rates, as well as poor prognosis. In vivo, ^{89}Zr-REGN3767 showed high specific uptake in human LAG-3-expressing M38 tumors in immunodeficient mice. In addition, LAG-3-positive T cells in the spleen could be detected.

Overall, these findings support the idea of LAG-3-based PET for the assessment of LAG-3 expression, with the goal to predict and monitor response to checkpoint blockade in the future.

CURRENT CLINICAL STATUS

While the above described studies evaluated these novel checkpoint imaging approaches in animal models, very recently, the first results on checkpoint-specific PET imaging in humans have been published.

Niemeijer et al. reported the first-in-human study of whole-body PET imaging with ^{89}Zr-nivolumab (anti-PD-1) (7 days postinjection) and ^{18}F-BMS-986192, an ^{18}F-labeled anti-PD-L1 Adnectin (1 h postinjection), in 13 patients with advanced NSCLC, prior to treatment with nivolumab (*80*). Both tracers showed adequate tumor-to-background contrast for tumor visualization. However, between patients, as well as between different tumor lesions, heterogeneous tracer uptake was reported for both tracers. ^{18}F-BMS-986192 uptake in tumor lesions correlated with tumor PD-L1 expression, measured by immunohistochemistry. ^{89}Zr-nivolumab uptake correlated with PD-1-expressing tumor-infiltrating immune cells. Both tracers showed high accumulation in the spleen, which the authors attribute to binding to PD-1 and PD-L1 receptors on lymphocytes and dendritic cells. Moreover, tracer uptake in the liver was observed, likely due to catabolism of the tracers. The smaller sized ^{18}F-BMS-986192 tracer mainly demonstrated biliary and renal excretion, while ^{89}Zr-Nivolumab was excreted via the gastrointestinal route, which is typical for monoclonal antibodies. Overall, for both tracers, the authors report a correlation between tracer uptake in the tumors and response to nivolumab treatment. In summary, these findings suggest that PD-1- and PD-L1-specific PET/CT imaging may be useful to non-invasively evaluate PD-1 and PD-L1 expression in patients with NSCLC.

Bensch at al. recently presented the initial results of a first-in-human study evaluating the ^{89}Zr-labeled anti-PD-L1 antibody atezolizumab in 22 patients with locally advanced or metastatic bladder cancer, NSCLC, or triple-negative breast cancer before the start of atezolizumab therapy with PET/CT

(*81*). The authors were able to show that the imaging signal corresponds with PD-L1 expression at sites of inflammation as well as in various normal lymphoid tissues. In tumors, high but heterogeneous uptake was observed, varying within and among lesions, patients, and tumor types (**figure 3**). Interestingly, for progression-free and overall survival, the tracer uptake appeared to be a strong predictor of response to atezolizumab treatment.

In yet another first-in human study, Xing et al. assessed the single domain anti-PD-L1 antibody NM-01, which was site-specifically labeled with ^{99m}Tc for SPECT imaging in 16 patients with NSCLC (*82*). The administered activity ranged from 3.8 – 10.4 MBq/kg body weight, corresponding to 100 or 400 µg of NM-01. Tracer uptake was observed in kidneys, spleen, liver, and bone marrow with acceptable radiation dosimetry profile. The different protein doses revealed no significant difference in tumor-to-background ratios. The authors conclude that ^{99m}Tc-NM-01-based SPECT is a safe diagnostic procedure delivering a tolerable radiation dose and has favorable biodistribution and image characteristics correlating with PD-L1 immunohistochemical stainings in patients with NSCLC.

SUMMARY AND OUTLOOK

In conclusion, in this review, an overview is provided on the recent developments in checkpoint imaging in oncology. So far, first evidence for non-invasive visualization of various targets for immune checkpoint blockade therapy has been provided using radiolabeled antibodies, antibody fragments, nanobodies, peptides and adnectins for SPECT and PET imaging. Besides pure a priori visualization of target expression levels in the tumor tissue, analysis of expression heterogeneity in and between tumor lesions has been reported. In addition, evidence for visualizing the infiltration of target-expressing T-cells into the tumor microenvironment as well as in healthy immune tissues was provided and checkpoint imaging was reported to allow monitoring of changes in target expression levels upon application of different treatments (radiotherapy, IFN-γ). Finally, first evidence suggests that checkpoint imaging may be used to predict responses to checkpoint blockade therapy.

So far, first clinical studies have been performed, mainly focusing on the visualization of PD-L1, showing encouraging results, and numerous clinical studies have been initiated with their results yet to come. However, prior to full clinical exploitation of checkpoint imaging, various aspects still have to be investigated. Among the variety of different targeting molecules being evaluated, consensus should be found on which tracers are most suitable to meet the clinical needs. This includes direct comparison between smaller-sized targeting molecules with intact IgG molecules for checkpoint imaging, together with selecting radioisotopes and chelating molecules optimally matching the pharmacokinetics of these targeting molecules. In addition, further studies should address in which situations imaging of the checkpoint receptor should be performed and in which situations the ligand should be targeted. Moreover, the impact of false-positive situations, such as in infections, which frequently are accompanied with influx of immune cells, should be evaluated.

Since visualization of immune cell infiltration was possible, applications of checkpoint imaging may not be limited to oncologic scenarios, but may also be applied in infectious or inflammatory situations and auto-immune conditions.

While checkpoint imaging is currently still in very early stages of development and many facets must be worked out before full clinical exploitation, the results obtained so far look very promising. Eventually, checkpoint imaging may help to optimize patient selection, predict and monitor responses to checkpoint blockade, and aid the development of novel combinatorial regimens to be applied in a personalized fashion to suit each patient's individual situation.

DISCLOSURE

The authors declare that no conflicts of interest exist.

KEY POINTS

Question

What ist he role of immune checkpoint imaging in oncology with respect to personalized patient care?

Pertinent findings

In this review article, an overview on the current developments in immune checkpoint imaging is provided. Various preclinical studies have shown proof-of-principle for visualizing target expression levels in the tumor tissue and infiltration of target-expressing immune cells into the tumor microenvironment. Checkpoint imaging was shown to be feasible for monitoring expression level changes upon treatment and it may be used to predict responses to checkpoint blockade therapy. Based on these promising findings, and numerous clinical studies have been initiated.

Implications for patient care

Immune checkpoint imaging may drastically improve patient selection and response evaluation in oncologic patients prior to, during, and after treatment with checkpoint inhibitors.

REFERENCES

1. Hanahan D, Weinberg RA. Hallmarks of cancer: the next generation. *Cell.* 2011;144:646-674.

2. Topalian SL, Hodi FS, Brahmer JR, et al. Safety, activity, and immune correlates of anti-PD-1 antibody in cancer. *N Engl J Med.* 2012;366:2443-2454.

3. Buchbinder EI, Desai A. CTLA-4 and PD-1 Pathways: Similarities, Differences, and Implications of Their Inhibition. *Am J Clin Oncol.* 2016;39:98-106.

4. Hodi FS, Chiarion-Sileni V, Gonzalez R, et al. Nivolumab plus ipilimumab or nivolumab alone versus ipilimumab alone in advanced melanoma (CheckMate 067): 4-year outcomes of a multicentre, randomised, phase 3 trial. *Lancet Oncology.* 2018;19:1480-1492.

5. Paz-Ares L, Brahmer J, Hellmann MD, et al. CheckMate 227: A randomized, open-label phase 3 trial of nivolumab, nivolumab plus ipilimumab, or nivolumab plus chemotherapy versus chemotherapy in hemotherapy-naive patients with advanced non-small cell lung cancer (NSCLC). *Annals of Oncology.* 2017;28.

6. Mok TSK, Wu YL, Kudaba I, et al. Pembrolizumab versus chemotherapy for previously untreated, PD-L1-expressing, locally advanced or metastatic non-small-cell lung cancer (KEYNOTE-042): a randomised, open-label, controlled, phase 3 trial. *Lancet.* 2019;393:1819-1830.

7. Mezquita L, Planchard D. Durvalumab for the treatment of non-small cell lung cancer. *Expert Review of Respiratory Medicine.* 2018;12:627-639.

8. Barlesi F, Vansteenkiste J, Spigel D. Avelumab versus docetaxel in patients with platinum-treated advanced non-small-cell lung cancer (JAVELIN Lung 200): an open-label, randomised, phase 3 study (vol 19, pg 1468, 2018). *Lancet Oncology.* 2018;19:E581-E581.

9. Rini BI, Powles T, Atkins MB, et al. Atezolizumab plus bevacizumab versus sunitinib in patients with previously untreated metastatic renal cell carcinoma (IMmotion151): a multicentre, open-label, phase 3, randomised controlled trial. *Lancet.* 2019;393:2404-2415.

10. Reck M, Rodriguez-Abreu D, Robinson AG, et al. Pembrolizumab versus Chemotherapy for PD-L1-Positive Non-Small-Cell Lung Cancer. *N Engl J Med.* 2016;375:1823-1833.

11. Naidoo J, Page DB, Li BT, et al. Toxicities of the anti-PD-1 and anti-PD-L1 immune checkpoint antibodies. *Ann Oncol.* 2015;26:2375-2391.

12. Freeman-Keller M, Kim Y, Cronin H, Richards A, Gibney G, Weber JS. Nivolumab in Resected and Unresectable Metastatic Melanoma: Characteristics of Immune-Related Adverse Events and Association with Outcomes. *Clin Cancer Res.* 2016;22:886-894.

13. Kazandjian D, Khozin S, Blumenthal G, et al. Benefit-Risk Summary of Nivolumab for Patients With Metastatic Squamous Cell Lung Cancer After Platinum-Based Chemotherapy: A Report From the US Food and Drug Administration. *JAMA Oncol.* 2016;2:118-122.

14. Keir ME, Butte MJ, Freeman GJ, Sharpe AH. PD-1 and its ligands in tolerance and immunity. *Annu Rev Immunol.* 2008;26:677-704.

15. He J, Hu Y, Hu M, Li B. Development of PD-1/PD-L1 Pathway in Tumor Immune Microenvironment and Treatment for Non-Small Cell Lung Cancer. *Sci Rep.* 2015;5:13110.

16. Taube JM, Young GD, McMiller TL, et al. Differential Expression of Immune-Regulatory Genes Associated with PD-L1 Display in Melanoma: Implications for PD-1 Pathway Blockade. *Clin Cancer Res.* 2015;21:3969-3976.

17. Motzer RJ, Escudier B, McDermott DF, et al. Nivolumab versus Everolimus in Advanced Renal-Cell Carcinoma. *N Engl J Med.* 2015;373:1803-1813.

18. Weber JS. Tumor evasion may occur via expression of regulatory molecules: a case for CTLA-4 in melanoma. *J Invest Dermatol.* 2008;128:2750-2752.

19. Shah KV, Chien AJ, Yee C, Moon RT. CTLA-4 is a direct target of Wnt/beta-catenin signaling and is expressed in human melanoma tumors. *J Invest Dermatol.* 2008;128:2870-2879.

20. Contardi E, Palmisano GL, Tazzari PL, et al. CTLA-4 is constitutively expressed on tumor cells and can trigger apoptosis upon ligand interaction. *Int J Cancer.* 2005;117:538-550.

21. Salvi S, Fontana V, Boccardo S, et al. Evaluation of CTLA-4 expression and relevance as a novel prognostic factor in patients with non-small cell lung cancer. *Cancer Immunol Immunother.* 2012;61:1463-1472.

22. Ehlerding EB, England CG, Majewski RL, et al. ImmunoPET Imaging of CTLA-4 Expression in Mouse Models of Non-small Cell Lung Cancer. *Mol Pharm.* 2017;14:1782-1789.

23. Antczak A, Pastuszak-Lewandoska D, Gorski P, et al. Ctla-4 expression and polymorphisms in lung tissue of patients with diagnosed non-small-cell lung cancer. *Biomed Res Int.* 2013;2013:576486.

24. Buchbinder E, Hodi FS. Cytotoxic T lymphocyte antigen-4 and immune checkpoint blockade. *J Clin Invest.* 2015;125:3377-3383.

25. Callahan MK, Wolchok JD. At the bedside: CTLA-4- and PD-1-blocking antibodies in cancer immunotherapy. *J Leukoc Biol.* 2013;94:41-53.

26. Kassardjian A, Shintaku PI, Moatamed NA. Expression of immune checkpoint regulators, cytotoxic T lymphocyte antigen 4 (CTLA-4) and programmed death-ligand 1 (PD-L1), in female breast carcinomas. *PLoS One.* 2018;13:e0195958.

27. Hodi FS, O'Day SJ, McDermott DF, et al. Improved survival with ipilimumab in patients with metastatic melanoma. *N Engl J Med.* 2010;363:711-723.

28. Wong ANM, McArthur GA, Hofman MS, Hicks RJ. The Advantages and Challenges of Using FDG PET/CT for Response Assessment in Melanoma in the Era of Targeted Agents and Immunotherapy. *Eur J Nucl Med Mol Imaging.* 2017;44:67-77.

29. Cho SY, Lipson EJ, Im HJ, et al. Prediction of Response to Immune Checkpoint Inhibitor Therapy Using Early-Time-Point (18)F-FDG PET/CT Imaging in Patients with Advanced Melanoma. *J Nucl Med.* 2017;58:1421-1428.

30. Takada K, Toyokawa G, Yoneshima Y, et al. 18F-FDG uptake in PET/CT is a potential predictive biomarker of response to anti-PD-1 antibody therapy in non-small cell lung cancer. *Scientific reports.* 2019;9:13362.

31. Bundschuh RA, Dinges J, Neumann L, et al. Textural Parameters of Tumor Heterogeneity in (1)(8)F-FDG PET/CT for Therapy Response Assessment and Prognosis in Patients with Locally Advanced Rectal Cancer. *J Nucl Med.* 2014;55:891-897.

32. Levine EA, Farmer MR, Clark P, et al. Predictive value of 18-fluoro-deoxy-glucose-positron emission tomography (18F-FDG-PET) in the identification of responders to chemoradiation therapy for the treatment of locally advanced esophageal cancer. *Annals of surgery.* 2006;243:472-478.

33. Rizk NP, Tang L, Adusumilli PS, et al. Predictive value of initial PET-SUVmax in patients with locally advanced esophageal and gastroesophageal junction adenocarcinoma. *Journal of thoracic oncology : official publication of the International Association for the Study of Lung Cancer.* 2009;4:875-879.

34. Werner RA, Ilhan H, Lehner S, et al. Pre-therapy Somatostatin Receptor-Based Heterogeneity Predicts Overall Survival in Pancreatic Neuroendocrine Tumor Patients Undergoing Peptide Receptor Radionuclide Therapy. *Mol Imaging Biol.* 2018.

35. Dong H, Strome SE, Salomao DR, et al. Tumor-associated B7-H1 promotes T-cell apoptosis: a potential mechanism of immune evasion. *Nat Med.* 2002;8:793-800.

36. Joseph RW, Parasramka M, Eckel-Passow JE, et al. Inverse association between programmed death ligand 1 and genes in the VEGF pathway in primary clear cell renal cell carcinoma. *Cancer Immunol Res.* 2013;1:378-385.

37. Kondo A, Yamashita T, Tamura H, et al. Interferon-gamma and tumor necrosis factor-alpha induce an immunoinhibitory molecule, B7-H1, via nuclear factor-kappaB activation in blasts in myelodysplastic syndromes. *Blood.* 2010;116:1124-1131.

38. Ghebeh H, Lehe C, Barhoush E, et al. Doxorubicin downregulates cell surface B7-H1 expression and upregulates its nuclear expression in breast cancer cells: role of B7-H1 as an anti-apoptotic molecule. *Breast Cancer Res.* 2010;12:R48.

39. Zhang P, Su DM, Liang M, Fu J. Chemopreventive agents induce programmed death-1-ligand 1 (PD-L1) surface expression in breast cancer cells and promote PD-L1-mediated T cell apoptosis. *Mol Immunol.* 2008;45:1470-1476.

40. Deng L, Liang H, Burnette B, et al. Irradiation and anti-PD-L1 treatment synergistically promote antitumor immunity in mice. *J Clin Invest.* 2014;124:687-695.

41. Scala S. Molecular Pathways: Targeting the CXCR4-CXCL12 Axis--Untapped Potential in the Tumor Microenvironment. *Clin Cancer Res.* 2015;21:4278-4285.

42. Callea M, Albiges L, Gupta M, et al. Differential Expression of PD-L1 between Primary and Metastatic Sites in Clear-Cell Renal Cell Carcinoma. *Cancer Immunol Res.* 2015;3:1158-1164.

43. Jilaveanu LB, Shuch B, Zito CR, et al. PD-L1 Expression in Clear Cell Renal Cell Carcinoma: An Analysis of Nephrectomy and Sites of Metastases. *J Cancer.* 2014;5:166-172.

44. Madore J, Vilain RE, Menzies AM, et al. PD-L1 expression in melanoma shows marked heterogeneity within and between patients: implications for anti-PD-1/PD-L1 clinical trials. *Pigment Cell Melanoma Res.* 2015;28:245-253.

45. Taube JM, Klein A, Brahmer JR, et al. Association of PD-1, PD-1 ligands, and other features of the tumor immune microenvironment with response to anti-PD-1 therapy. *Clin Cancer Res.* 2014;20:5064-5074.

46. Fusi A, Festino L, Botti G, et al. PD-L1 expression as a potential predictive biomarker. *Lancet Oncol.* 2015;16:1285-1287.

47. Ilie M, Long-Mira E, Bence C, et al. Comparative study of the PD-L1 status between surgically resected specimens and matched biopsies of NSCLC patients reveal major discordances: a potential issue for anti-PD-L1 therapeutic strategies. *Ann Oncol.* 2016;27:147-153.

48. Muller P, Rothschild SI, Arnold W, et al. Metastatic spread in patients with non-small cell lung cancer is associated with a reduced density of tumor-infiltrating T cells. *Cancer Immunol Immunother.* 2016;65:1-11.

49. Heskamp S, Hobo W, Molkenboer-Kuenen JD, et al. Noninvasive Imaging of Tumor PD-L1 Expression Using Radiolabeled Anti-PD-L1 Antibodies. *Cancer Res.* 2015;75:2928-2936.

50. Chatterjee S, Lesniak WG, Gabrielson M, et al. A humanized antibody for imaging immune checkpoint ligand PD-L1 expression in tumors. *Oncotarget.* 2016;7:10215-10227.

51. Truillet C, Oh HLJ, Yeo SP, et al. Imaging PD-L1 Expression with ImmunoPET. *Bioconjugate Chemistry.* 2018;29:96-103.

52. Heskamp S, Wierstra PJ, Molkenboer-Kuenen JDM, et al. PD-L1 microSPECT/CT Imaging for Longitudinal Monitoring of PD-L1 Expression in Syngeneic and Humanized Mouse Models for Cancer. *Cancer Immunol Res.* 2019;7:150-161.

53. Josefsson A, Nedrow JR, Park S, et al. Imaging, Biodistribution, and Dosimetry of Radionuclide-Labeled PD-L1 Antibody in an Immunocompetent Mouse Model of Breast Cancer. *Cancer Res.* 2016;76:472-479.

54. Nedrow JR, Josefsson A, Park S, Ranka S, Roy S, Sgouros G. Imaging of Programmed Cell Death Ligand 1: Impact of Protein Concentration on Distribution of Anti-PD-L1 SPECT Agents in an Immunocompetent Murine Model of Melanoma. *J Nucl Med.* 2017;58:1560-1566.

55. Hettich M, Braun F, Bartholoma MD, Schirmbeck R, Niedermann G. High-Resolution PET Imaging with Therapeutic Antibody-based PD-1/PD-L1 Checkpoint Tracers. *Theranostics.* 2016;6:1629-1640.

56. Jagoda EM, Vasalatiy O, Basuli F, et al. Immuno-PET Imaging of the Programmed Cell Death-1 Ligand (PD-L1) Using a Zirconium-89 Labeled Therapeutic Antibody, Avelumab. *Mol Imaging.* 2019;18:1536012119829986.

57. Lesniak WG, Chatterjee S, Gabrielson M, et al. PD-L1 Detection in Tumors Using [(64)Cu]Atezolizumab with PET. *Bioconjug Chem.* 2016;27:2103-2110.

58. Rinne SS, Leitao CD, Mitran B, et al. Optimization of HER3 expression imaging using affibody molecules: Influence of chelator for labeling with indium-111. *Sci Rep.* 2019;9:655.

59. Kikuchi M, Clump DA, Srivastava RM, et al. Preclinical immunoPET/CT imaging using Zr-89-labeled anti-PD-L1 monoclonal antibody for assessing radiation-induced PD-L1 upregulation in head and neck cancer and melanoma. *Oncoimmunology.* 2017;6:e1329071.

60. Ehlerding EB, Lee HJ, Barnhart TE, et al. Noninvasive Imaging and Quantification of Radiotherapy-Induced PD-L1 Upregulation with (89)Zr-Df-Atezolizumab. *Bioconjug Chem.* 2019;30:1434-1441.

61. Li D, Cheng SY, Zou SJ, et al. Immuno-PET Imaging of Zr-89 Labeled Anti-PD-L1 Domain Antibody. *Molecular Pharmaceutics.* 2018;15:1674-1681.

62. Wissler HL, Ehlerding EB, Lyu Z, et al. Site-Specific Immuno-PET Tracer to Image PD-L1. *Mol Pharm.* 2019;16:2028-2036.

63. Broos K, Keyaerts M, Lecocq Q, et al. Non-invasive assessment of murine PD-L1 levels in syngeneic tumor models by nuclear imaging with nanobody tracers. *Oncotarget.* 2017;8:41932-41946.

64. Lv G, Qiu L, Sun Y, et al. PET imaging of tumor PD-L1 expression with a highly specific non-blocking nanobody. *J Nucl Med.* 2019.

65. Trotter DEG, Meng XJ, McQuade P, et al. In Vivo Imaging of the Programmed Death Ligand 1 by F-18 PET. *Journal of Nuclear Medicine.* 2017;58:1852-1857.

66. Donnelly DJ, Smith RA, Morin P, et al. Synthesis and Biologic Evaluation of a Novel F-18-Labeled Adnectin as a PET Radioligand for Imaging PD-L1 Expression. *Journal of Nuclear Medicine.* 2018;59:529-535.

67. Chatterjee S, Lesniak WG, Miller MS, et al. Rapid PD-L1 detection in tumors with PET using a highly specific peptide. *Biochem Biophys Res Commun.* 2017;483:258-263.

68. De Silva RA, Kumar D, Lisok A, et al. Peptide-Based Ga-68-PET Radiotracer for Imaging PD-L1 Expression in Cancer. *Molecular Pharmaceutics.* 2018;15:3946-3952.

69. Lesniak WG, Mease RC, Chatterjee S, et al. Development of [(18)F]FPy-WL12 as a PD-L1 Specific PET Imaging Peptide. *Mol Imaging.* 2019;18:1536012119852189.

70. Muenst S, Soysal SD, Gao F, Obermann EC, Oertli D, Gillanders WE. The presence of programmed death 1 (PD-1)-positive tumor-infiltrating lymphocytes is associated with poor prognosis in human breast cancer. *Breast Cancer Res Treat.* 2013;139:667-676.

71. Natarajan A, Mayer AT, Xu L, Reeves RE, Gano J, Gambhir SS. Novel Radiotracer for ImmunoPET Imaging of PD-1 Checkpoint Expression on Tumor Infiltrating Lymphocytes. *Bioconjug Chem.* 2015;26:2062-2069.

72. Cole EL, Kim J, Donnelly DJ, et al. Radiosynthesis and preclinical PET evaluation of (89)Zr-nivolumab (BMS-936558) in healthy non-human primates. *Bioorg Med Chem.* 2017;25:5407-5414.

73. England CG, Jiang D, Ehlerding EB, et al. (89)Zr-labeled nivolumab for imaging of T-cell infiltration in a humanized murine model of lung cancer. *Eur J Nucl Med Mol Imaging.* 2018;45:110-120.

74. England CG, Ehlerding EB, Hernandez R, et al. Preclinical Pharmacokinetics and Biodistribution Studies of 89Zr-Labeled Pembrolizumab. *J Nucl Med.* 2017;58:162-168.

75. Natarajan A, Mayer AT, Reeves RE, Nagamine CM, Gambhir SS. Development of Novel ImmunoPET Tracers to Image Human PD-1 Checkpoint Expression on Tumor-Infiltrating Lymphocytes in a Humanized Mouse Model. *Mol Imaging Biol.* 2017;19:903-914.

76. Wolchok JD, Weber JS, Maio M, et al. Four-year survival rates for patients with metastatic melanoma who received ipilimumab in phase II clinical trials. *Ann Oncol.* 2013;24:2174-2180.

77. Ehlerding EB, Lee HJ, Jiang D, et al. Antibody and fragment-based PET imaging of CTLA-4+ T-cells in humanized mouse models. *Am J Cancer Res.* 2019;9:53-63.

78. Kelly MP, Tavare R, Giurleo JT, et al. Immuno-PET detection of LAG-3 expressing intratumoral lymphocytes using the zirconium-89 radiolabeled fully human anti-LAG-3 antibody REGN3767. *Cancer Research.* 2018;78.

79. Burugu S, Gao D, Leung S, Chia SK, Nielsen TO. LAG-3+ tumor infiltrating lymphocytes in breast cancer: clinical correlates and association with PD-1/PD-L1+ tumors. *Ann Oncol.* 2017;28:2977-2984.

80. Niemeijer AN, Leung D, Huisman MC, et al. Whole body PD-1 and PD-L1 positron emission tomography in patients with non-small-cell lung cancer. *Nat Commun.* 2018;9:4664.

81. Bensch F, van der Veen EL, Lub-de Hooge MN, et al. (89)Zr-atezolizumab imaging as a non-invasive approach to assess clinical response to PD-L1 blockade in cancer. *Nat Med.* 2018;24:1852-1858.

82. Xing Y, Chand G, Liu C, et al. Early Phase I Study of a (99m)Tc-Labeled Anti-Programmed Death Ligand-1 (PD-L1) Single-Domain Antibody in SPECT/CT Assessment of PD-L1 Expression in Non-Small Cell Lung Cancer. *J Nucl Med.* 2019;60:1213-1220.

Table 1: Overview of the currently available preclinical checkpoint imaging studies

Targeting molecule	Radio-isotope	Chelator	Animal model	Tumor model	Accumulation time	Group
PD-L1						
Murine mAb PD-L1.3.1	^{111}In	DTPA	BALB/c nude mice	MDA-MB-231, SK-Br-3, SUM149, MCF-7, BT474	0, 1, 3, 7 d	Heskamp et al., 2015
Atezolizumab	^{111}In	DTPA	NSG mice	CHO-PDL1, CHO, H2444, H1155, MDA-MB-231, SUM149	24, 48, 72, 96, 120 h	Chatterjee et al., 2016
Murine anti-PD-L1 antibody	^{111}In	DTPA	Neu-N transgenic mice	NT2.5	72 h	Josefsson et al., 2016
Anti-mouse PD-L1 antibody	^{111}In	DTPA	C57BL/6 mice	B16F10	24, 72 h	Nedrow et al., 2017
Anti-murine anti-PD-L1 antibody α-PD-L1 (10F.9G2)	^{64}Cu	NOTA	C57BL/6N mice	B16F10	24 h	Hettich et al., 2016
Anti-PD-L1 antibody C4	^{89}Zr	DFO	nu/nu mice, C57 BL/6J mice	H1975, PC3, A549	8, 24, 48, 72, and 120 h	Truillet et al., 2018
Atezolizumab	^{64}Cu	DOTAGA	NSG mice	CHO-hPD-L1, MDA-MB-231, CHO, SUM149	24, 48 h	Lesniak et al, 2016
Avelumab	^{89}Zr	DFO	Athymic nude mice	MDA-MB-231	1, 2, 3, 6 d	Jagoda et al., 2019
Anti-murine anti-PD-L1 antibody 10F.9G2	^{89}Zr	DFO	C57BL/6 mice	MEER, B16F10	48 h + 96 h	Kikuchi et al., 2017
Anti-hPD-L1, clone PD-L1.3.1, anti-mPD-L1, clone 10F.9G2	^{111}In	DTPA	BALB/c, C57BL/6, and NSG mice	Renca, 4T1, CT26, B16F1, LLC1	1, 3, 7 d	Heskamp et al., 2019
Atezolizumab	^{89}Zr	Df	Athymic nude mice	H460, A549	1, 6, 12, 24, 48, 72, 96 h	Ehlerding et al., 2019
ZPD L1_1 affibody	^{18}F-AlF	NOTA	SCID beige mice	LOX, SUDHL6	30–90 min	González Trotter et al., 2017
KN035 domain antibody containing Fc tail fused to two single domains (anti-human PD-L1)	^{89}Zr	DFO	BALB/c nude mice, non-human primates	LN229	1, 6, 24, 48, 72, 120 h	Li et al., 2018
PD-L1 specific Fab fragment	^{64}Cu	NOTA	Athymic nude mice	-	5, 15, 45 min	Wissler et al., 2019
Anti-PD-L1 adnectin BMS-986192	^{18}F		Athymic nude mice	HT-29, L2987	90–120 min	Donnelly et al. 2018
Peptide WL12	^{64}Cu	DOTAGA	NSG mice	CHO, hPD-L1	10, 30, 60, 120 min	Chatterjee et al., 2017
Peptide WL12	^{68}Ga	DOTAGA	NSG mice	hPD-L1, CHO, MDA-MB-231, SUM149	15, 60, 120 min	De Silva et al., 2018
Peptide WL12	^{18}F		NSG mice	hPD-L1, CHO, H226, H1155, MDA-MB-231, SUM149	10, 60, 120 min	Lesniak et al., 2019
Nanobodies C3, C7, E2 and E4	^{99m}Tc		C57BL/6 mice	HEK293T	1 h	Broos et al., 2017
Nanobody Nb109	^{68}Ga	NOTA	BALB/c nude mice	A375-hPD-L1, MCF-7	1, 2, 4 h	Lv et al., 2019
PD-1						
Anti-PD-1 antibody	^{64}Cu	DOTA	Foxp3+.LuciDTR4 mice	B16F10	48 h	Natarajan et al., 2015
Anti-PD-1 antibody	^{64}Cu	NOTA	C57BL/6 mice	B16F10	24 h	Hettich et al., 2016
Nivolumab	^{89}Zr	DFO	Cynomolgus non-human primates	-	1, 4, 6, 8 d	Cole et al., 2017
Nivolumab	^{89}Zr	Df	NSG mice	A549	3, 6, 12, 24, 48, 72, 168 h	England et al., 2018
Pembrolizumab	^{89}Zr	Df	ICR (CD-1), SCID, and NSG mice and Sprague–Dawley outbred rats	-	0.5, 6, 12, 24, 48, 72, 120, 168 h	England et al. 2017
Pembrolizumab	^{89}Zr ^{64}Cu	DOTA	NSG mice	A375	1, 4, 18, 24, 48, 72, 96, 120, 144 h	Natarjan et al., 2017
CTLA-4						
Ipilimumab	^{64}Cu	DOTA	Athymic nude mice	A549, H358	48 h	Ehlerding et al., 2017
Ipilimumab and F(ab´)$_2$ fragment of ipilimumab	^{64}Cu	NOTA	Humanized NBSGW mice	-	0.5, 3, 12, 24, 48 h	Ehlerding et al., 2019
LAG-3						
Fully human antibody REGN3767	^{89}Zr	DFO	Immunodeficient mice	MC38	6 d	Kelly et al., 2018

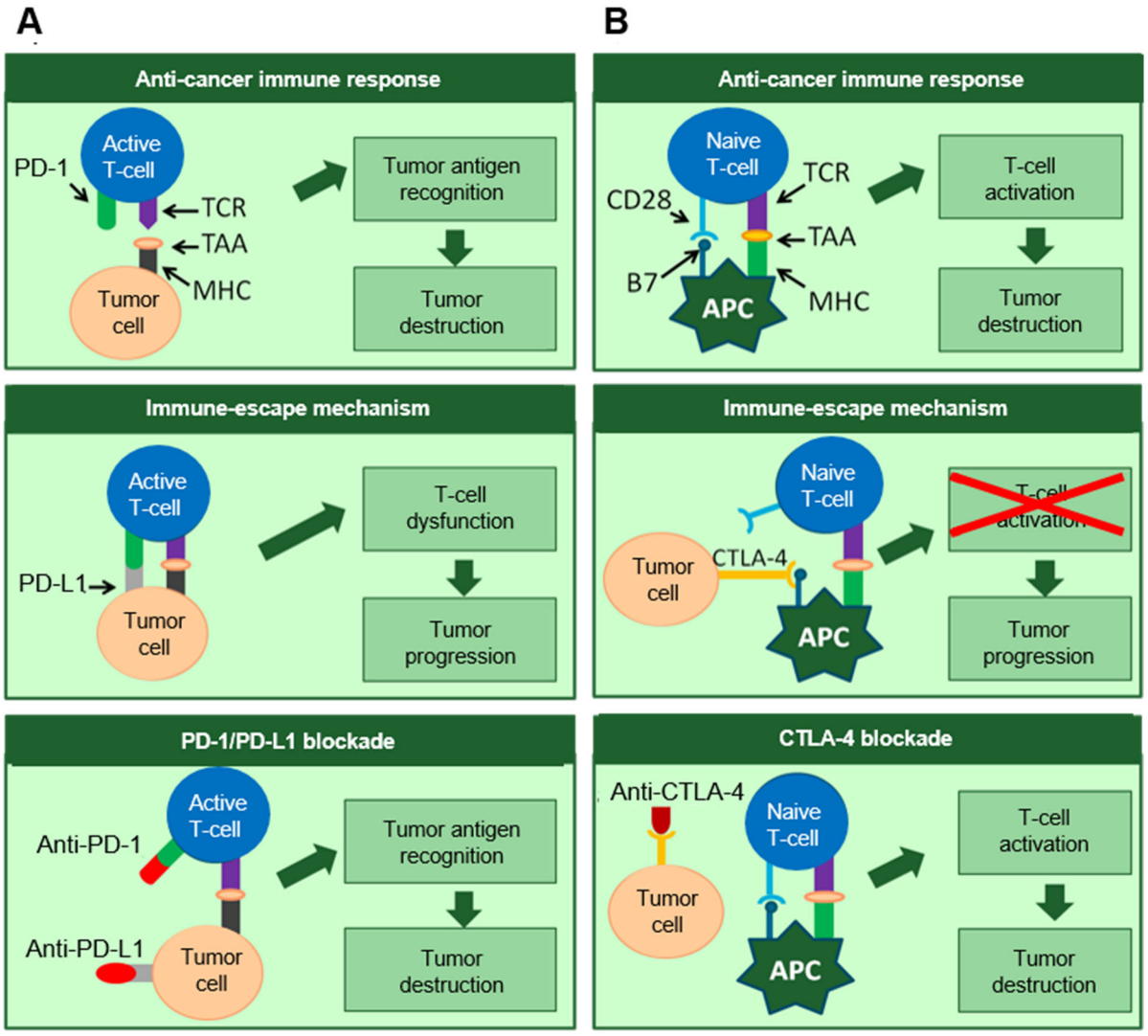

Figure 1: Simplified schematic representation of the PD-1 (A) and CTLA-4 (B) pathway and the mechanism of blocking these pathways. Abbreviations: TCR (T-cell receptor), TAA (tumor-associated antigen), MHC (major histocompatibility complex).

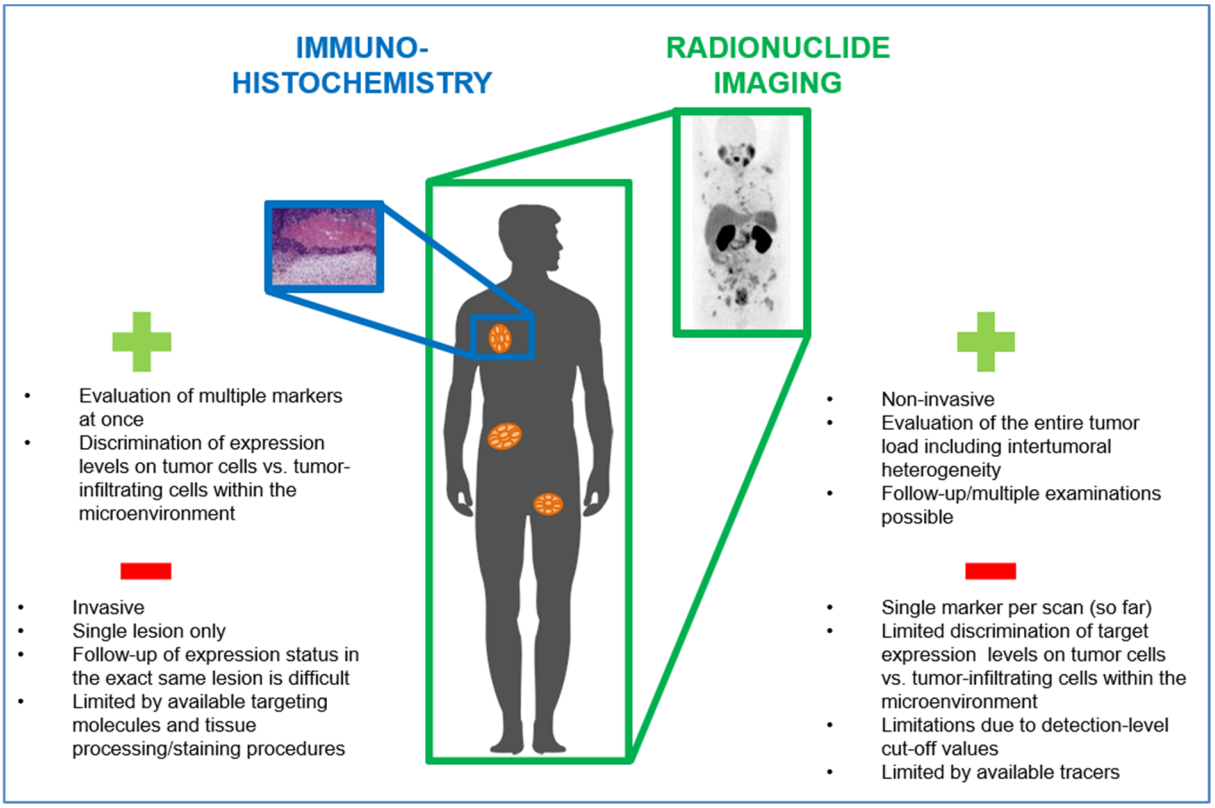

Figure 2: Schematic representation of the advantages and limitations of immunohistochemical analysis of checkpoint expression levels versus checkpoint imaging.

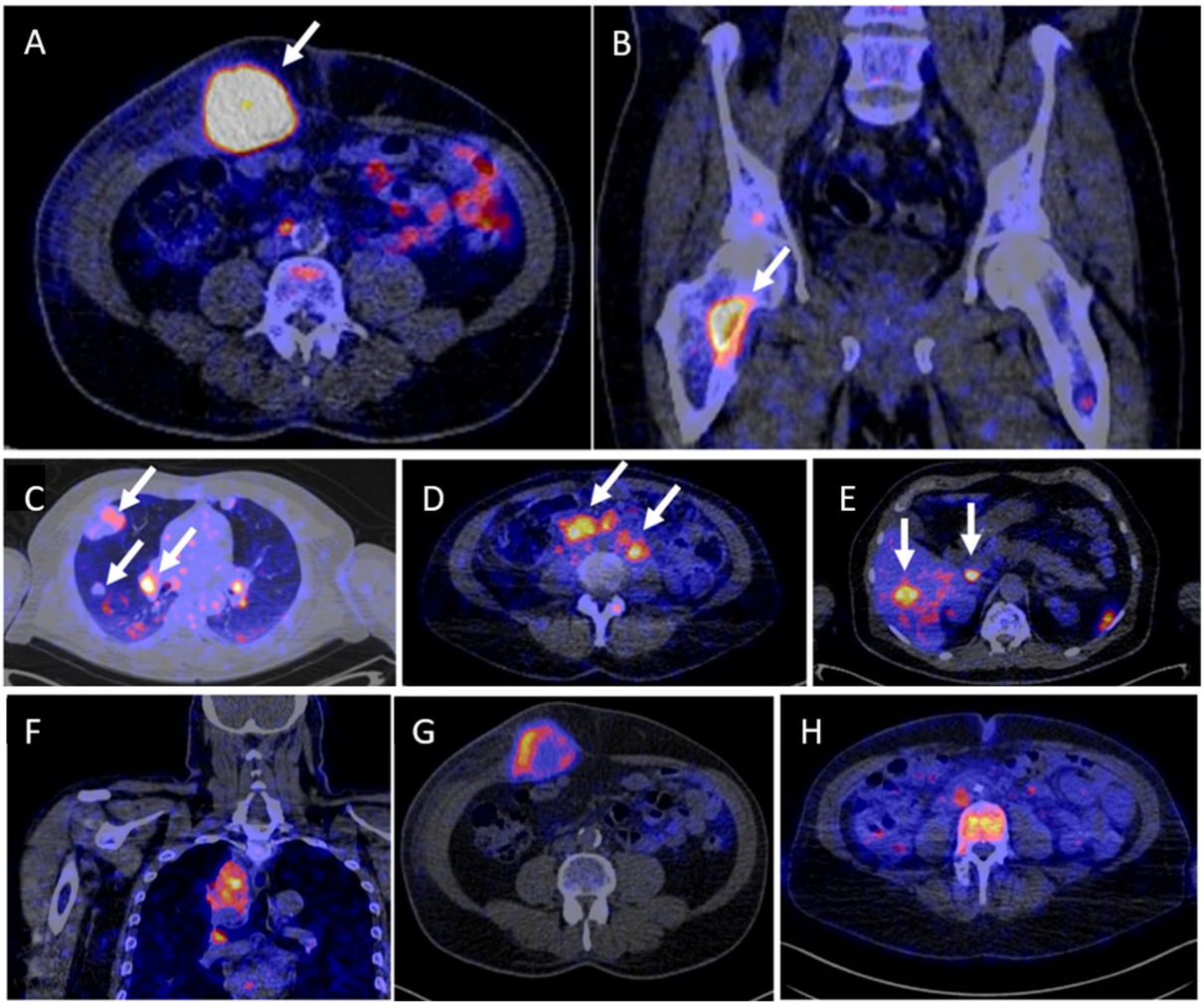

Figure 3: PET/CT images of four patients illustrating ^{89}Zr-atezolizumab tumor uptake in five different locations on day 7 postinjection (white arrows indicate tumor lesions) (A-E). PET/CT images of lesions of three patients with heterogeneous intralesional ^{89}Zr-atezolizumab uptake on day 7 postinjection (F-G). Mediastinal lesion of a NSCLC patient (SUV_{max} 19.9) (F), an abdominal wall metastases of a bladder cancer patient (SUV_{max} 36.4) (G), and a bone metastasis of a breast cancer patient (SUV_{max} 7.1) (H). This figure was adapted from Bensch et al. Nat Med. 2018 Dec;24(12):1852-1858 with permission of Nature Medicine.